Hindawi
Shock and Vibration
Volume 2018, Article ID 9496026, 8 pages
https://doi.org/10.1155/2018/9496026

Research Article

Design of a Submarine Vehicle for Higher Natural Frequency Using U^* Index Theory Approach

Weiyan Shang[1] and Qingguo Wang[2]

[1]*Department of Mechanical Engineering, Ningbo University of Technology, Ningbo, Zhejiang 315016, China*
[2]*Department of Mechanical Engineering, University of Manitoba, Winnipeg, Manitoba, Canada R3T 2N2*

Correspondence should be addressed to Qingguo Wang; qingguo.wang1984@gmail.com

Received 22 June 2018; Revised 15 September 2018; Accepted 18 September 2018; Published 23 October 2018

Academic Editor: Marco Gherlone

The natural frequency of a vehicle structure should be far higher than the road excitation frequency in order to avoid dynamic problems caused by structural resonance. Submarine vehicles or robots are facing the same issue as mentioned above. This paper proposed a means to effectively increase the natural frequency of submarine vehicles or robots by using U^* index approach. The U^* theory was originally introduced to investigate load transfer paths within a structure. It is a new design paradigm for vehicle structures. In this study, the U^* index theory was applied to evaluate the internal stiffness distribution of a submarine vehicle structure and then a modified design was achieved based on the U^* analysis. Compared to the original design, the natural frequency of the modified vehicle structure was increased by more than 40% while the weight of the modified vehicle was only raised by 4.6%.

1. Introduction

Recently, ocean engineering technologies have increasingly been focused by many countries and areas of the world. Submarine vehicles or robots are important to the investigation of ocean ecosystem, exploration of ocean energy, and heath monitoring of ocean platform and submarine pipelines. However, compared to ground vehicles, the development of design and manufacturing techniques of submarine vehicles are still in their primary stage [1]. Structural vibration and control is always one of the principal problems in vehicle design which significantly affects structural performance such as structural strength, durability, kinematic accuracy, and dynamic stability [2, 3]. To minimize the dynamic problems caused by the road excitation, natural frequency of ground vehicles needs to be far higher than 10–20 Hz which is a typical road excitation frequency [3]. To avoid the resonance phenomena, reasonable matching of stiffness between different parts or assemblies is also necessary in vehicle design [2]. Although road excitation data from the seabed are limited to date, a means to design submarine vehicles or robots with higher natural frequencies is imperative.

Structural stiffness is a determinant of modal shapes and frequencies of a structure. However, traditional finite element analysis (FEA) only gives structural stresses and displacements instead of a stiffness distribution. U^* index theory which was firstly introduced by Takahashi in 2005 is a method to investigate stiffness distribution of a structure [4]. The original purpose for proposing the U^* theory method is to calculate load transfer paths of a load-bearing structure. Load paths analysis is essential for designing better engineering structures in both mechanical performance and weight efficiency [5]. The U^* index theory was initially proposed to solve static and linear elastic problems. Recently, the U^* index theory has been extended to dynamic loads [6], nonlinear elasticity, composite materials [7], and six degrees of freedom systems [8]. Load paths analysis based on the U^* index theory is a new design paradigm because it can provide useful information for decision-making which cannot be achieved from traditional finite element analysis (FEA) [9]. The U^* theory has been applied in vehicle design

by automotive manufacturers like Honda and Nissan [10, 11].

In this paper, instead of load paths analysis, the U^* index theory was applied as a means to increase the natural frequency of submarine vehicles or robots to reduce the dynamic problems caused by excitations with lower frequencies. A submarine vehicle designed by our research group was used as the sample structure to demonstrate the effectiveness of the proposed method. Firstly, the internal relative stiffness distribution of the submarine vehicle structure was computed by the U^* index theory. Then, a U^*-based design criterion was employed to improve the overall stiffness of the submarine vehicle structure by only adding a small amount of mass. Finally, due to the improvement of the stiffness distribution, the natural frequency of the submarine vehicle structure was raised by 43.5% while the structural weight was only increased by 4.6%.

In the following parts of the paper, the U^* index theory and the U^*-based design criterion are presented in Section 2; the computational design method of the submarine vehicle structure is introduced in Section 3; the computational results of both original and modified designs are compared in Section 4; and the conclusion of the paper is drawn in Section 5.

2. Theoretical Preliminary: U^* Index Theory

Figure 1(a) shows a linear elastic body with the loading point A, supporting point B, and an arbitrary point C. The beams represent the internal stiffness between any two points of the system. The internal stiffness is the coupling stiffness between two specific points, whose meaning is totally different from the stiffness matrix in FEA. The following equation describes the force-displacement relationship among points A, B, and C:

$$\begin{bmatrix} \mathbf{F}_A \\ \mathbf{F}_B \\ \mathbf{F}_C \\ \mathbf{M}_A \\ \mathbf{M}_B \\ \mathbf{M}_C \end{bmatrix} = \begin{bmatrix} \mathbf{K}_{AA}^T & \cdots & \mathbf{K}_{AC}^T & \mathbf{K}_{AA}^{TR} & \cdots & \mathbf{K}_{AC}^{TR} \\ \vdots & \ddots & \vdots & \vdots & \ddots & \vdots \\ \mathbf{K}_{CA}^T & \cdots & \mathbf{K}_{CC}^T & \mathbf{K}_{CA}^{TR} & \cdots & \mathbf{K}_{CC}^{TR} \\ \mathbf{K}_{AA}^{RT} & \cdots & \mathbf{K}_{AC}^{RT} & \mathbf{K}_{AA}^{R} & \cdots & \mathbf{K}_{AC}^{R} \\ \vdots & \ddots & \vdots & \vdots & \ddots & \vdots \\ \mathbf{K}_{CA}^{RT} & \cdots & \mathbf{K}_{CC}^{RT} & \mathbf{K}_{CA}^{R} & \cdots & \mathbf{K}_{CC}^{R} \end{bmatrix} \begin{bmatrix} \mathbf{D}_A \\ \mathbf{D}_B \\ \mathbf{D}_C \\ \mathbf{R}_A \\ \mathbf{R}_B \\ \mathbf{R}_C \end{bmatrix}, \quad (1)$$

where $\mathbf{F}_{i(i=A,B,C)}$, $\mathbf{M}_{i(i=A,B,C)}$, $\mathbf{D}_{i(i=A,B,C)}$, and $\mathbf{R}_{i(i=A,B,C)}$ are all three-dimensional vectors representing forces, bending moments, translations, and rotations, respectively. $\mathbf{K}_{ij(i=A,B,C;j=A,B,C)}^T$, $\mathbf{K}_{ij(i=A,B,C;j=A,B,C)}^R$, $\mathbf{K}_{ij(i=A,B,C;j=A,B,C)}^{TR}$, and $\mathbf{K}_{ij(i=A,B,C;j=A,B,C)}^{RT}$ are the internal stiffness tensors, and they, respectively, characterize the relationships between forces and translations, moments and rotations, forces and rotations, and moments and translations.

In Figure 1(a), since point B is fixed ($D_B = R_B = 0$),

$$\mathbf{F}_A = \mathbf{K}_{AA}^T \mathbf{D}_A + \mathbf{K}_{AC}^T \mathbf{D}_C + \mathbf{K}_{AA}^{TR} \mathbf{R}_A + \mathbf{K}_{AC}^{TR} \mathbf{R}_C, \quad (2)$$

$$\mathbf{M}_A = \mathbf{K}_{AA}^{RT} \mathbf{D}_A + \mathbf{K}_{AC}^{RT} \mathbf{D}_C + \mathbf{K}_{AA}^{R} \mathbf{R}_A + \mathbf{K}_{AC}^{R} \mathbf{R}_C. \quad (3)$$

The external work of the system caused by the force $\mathbf{F}_A$ and the bending moment $\mathbf{M}_A$ is presented in Equations (4) and (5), respectively:

$$W_F = \frac{1}{2}\mathbf{F}_A \cdot \mathbf{D}_A = \frac{1}{2}\left(\mathbf{K}_{AA}^T \mathbf{D}_A + \mathbf{K}_{AC}^T \mathbf{D}_C + \mathbf{K}_{AA}^{TR} \mathbf{R}_A + \mathbf{K}_{AC}^{TR} \mathbf{R}_C\right) \cdot \mathbf{D}_A, \quad (4)$$

$$W_M = \frac{1}{2}\mathbf{M}_A \cdot \mathbf{R}_A = \frac{1}{2}\left(\mathbf{K}_{AA}^{RT} \mathbf{D}_A + \mathbf{K}_{AC}^{RT} \mathbf{D}_C + \mathbf{K}_{AA}^{R} \mathbf{R}_A + \mathbf{K}_{AC}^{R} \mathbf{R}_C\right) \cdot \mathbf{R}_A. \quad (5)$$

Figure 1(b) shows the arbitrary point C ($D_C = R_C = 0$) of the system is restrained while same displacements D_A and R_A are applied at point A. Equations (6) and (7) indicate the external work of the constrained system induced by the force $\mathbf{F}_A'$ and the bending moment $\mathbf{M}_A'$, respectively:

$$W_F' = \frac{1}{2}\mathbf{F}_A' \cdot \mathbf{D}_A = \frac{1}{2}\left(\mathbf{K}_{AA}^T \mathbf{D}_A + \mathbf{K}_{AA}^{TR} \mathbf{R}_A\right) \cdot \mathbf{D}_A, \quad (6)$$

$$W_M' = \frac{1}{2}\mathbf{M}_A' \cdot \mathbf{R}_A = \frac{1}{2}\left(\mathbf{K}_{AA}^{RT} \mathbf{D}_A + \mathbf{K}_{AA}^{R} \mathbf{R}_A\right) \cdot \mathbf{R}_A. \quad (7)$$

The U^* index under six DOFs is defined as

$$U^* = 1 - \frac{U}{U'} = 1 - \frac{W_F + W_M}{W_F' + W_M'}, \quad (8)$$

where U is the total strain energy of the original system (Figure 1(a)) and U' is the total strain energy of the constrained system (Figure 1(b)). Here, the total strain energy of the system is transformed from the external work [12].

Equation (8) can be rewritten as

$$1 - \frac{W_F + W_M}{W_F' + W_M'} = \left[-\frac{W_F' + W_M'}{(W_F + W_M) - (W_F' + W_M')}\right]^{-1}. \quad (9)$$

By subtracting 1 and then adding 1, Equation (9) equals to

$$\left[-\frac{W_F' + W_M'}{(W_F + W_M) - (W_F' + W_M')} - \frac{(W_F + W_M) - (W_F' + W_M')}{(W_F + W_M) - (W_F' + W_M')} + 1\right]^{-1} = \left[1 - \frac{W_F + W_M}{(W_F + W_M) - (W_F' + W_M')}\right]^{-1}. \quad (10)$$

By substituting Equations (4)–(7) into Equation (10), we get

$$U^* = \left[1 - \frac{2W_F + 2W_M}{(\mathbf{K}_{AC}^T \mathbf{D}_C) \cdot \mathbf{D}_A + (\mathbf{K}_{AC}^{TR} R_C) \cdot \mathbf{D}_A + (\mathbf{K}_{AC}^{RT} \mathbf{D}_C) \cdot \mathbf{R}_A + (\mathbf{K}_{AC}^{R} \mathbf{R}_C) \cdot \mathbf{R}_A}\right]^{-1}. \quad (11)$$

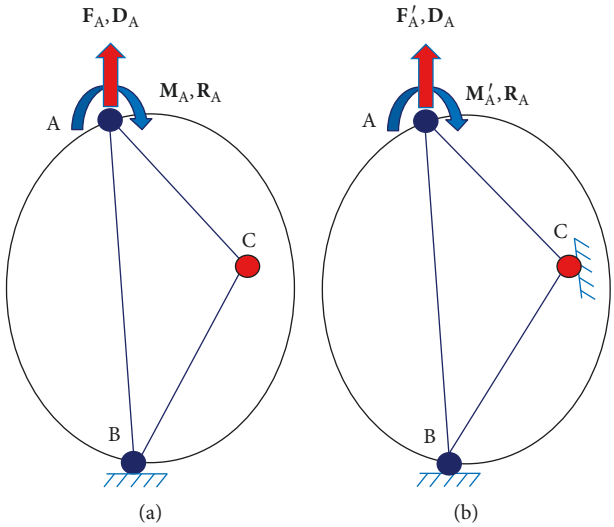

FIGURE 1: Calculation of the U^* index: (a) original system; (b) constrained system [8].

It can be seen from Equation (11) that the U^* index can be expressed in terms of the internal stiffness between the loading point and the arbitrary point of the system. In a structure, forces are mainly transferred through the stiffest parts in series with the loading point. Therefore, the lines with the highest U^* values (i.e., the ridge line of the U^* distribution) is defined as the main load paths. If a vector $\mathbf{g}^{(-)}$ is defined as

$$\mathbf{g}^{(-)} = -\text{grad}\, U^*, \tag{12}$$

the main load path is the line with the smallest $\mathbf{g}^{(-)}$. The vector $\mathbf{g}^{(-)}$ is regarded as the "stiffness decay vector" [11]. Figures 2(a) and 2(b) elaborate U^* and von Mises stress distributions of a plate with a hole, respectively. The solid black lines shown in Figure 2(a) are the main load paths predicted by the U^* index, which satisfy the expectation form the engineering point of view. As can be seen in Figure 2(b), the higher stresses are formed in the vicinity of the hole. However, since the hole is not important in transferring the forces, it is unreasonable to conclude the main load paths pass the locations with those higher stresses.

Normally, the U^* index decreases from the maximum value of one (1) at the loading point to the minimum value of zero (0) at the supporting point. In Figure (3), the solid line elaborates the variation of the U^* index along a path of a load-bearing structure and the dashed line depicts the U^* variation of the desirable condition. A uniform decay of the U^* index means the structural stiffness distribution is perfect, whereas, in reality, the U^* variation is nonuniform because of the structural issues. An increase or decrease of the rate of the U^* decay indicates that the stiffness in the corresponding part is higher or lower than other parts. The uniformity of the U^* decay is defined as the criterion to evaluate the rationality of the stiffness distribution of the structure. Structural modifications are required when the U^* curve is not uniform such as the solid line in Figure 3. The effective structural modifications shall reduce the shade area shown in Figure 3.

3. Computational Design Method

There are mainly three steps in the proposed computational design method. Firstly, a dynamic model is built, and a modal analysis is conducted on the vehicle structure. This is to obtain the natural frequency of the original design. Then, the vehicle structure is evaluated by using the U^*-based design criterion, while modification directions are suggested based on the U^* analysis. Thirdly, the natural frequency is recalculated to see the improvement from the design modification. If extra improvement is expected, the above procedures would be repeated until the result is desired.

Figure 4 shows the sample structure, a submarine vehicle (or robot) designed by our research group, which is used to demonstrate the usefulness of the proposed computational design method. The duties of the submarine vehicle are investigations of seabed ecosystems and explorations of ocean energy. Hence, minimizing the dynamic problems can effectively improve the accuracy and stability of data collection and dynamic control to the submarine vehicle. In the current study, the dynamic analysis and the design modification focuse on the vehicle suspension system. The material properties of the major components of the vehicle are given in Table 1.

Figure 5 illustrates the dynamic model of the submarine vehicle for modal analysis. The model is created in commercial FEA code ANSYS (release 18). The dynamic model includes the vehicle body and the major parts of the suspension system ignoring the crawler belt systems and the propellers. The properties of each component of the dynamic model are elaborated in Table 1. The boundary conditions can also be seen from Figure 5, where all the wheel holes in the vertical section of the suspension are fully constrained. All the components in the FEA model are modeled using Shell 181 Element with full integration. The block Lanczos method is selected as the mode extraction method [13].

Figure 6 demonstrates the static computer model for U^* calculation of the vehicle suspension system. In this model, the vehicle body is not included because the U^* analysis focuses on the load transfer behavior of the vehicle suspension system. The body weight of the vehicle body component is applied to the vehicle suspension system as the external force. The boundary conditions are the same as the dynamic model shown in Figure 6. The U^* analysis gives how the force of the vehicle body gravity is transferred through the vehicle suspension system. Meanwhile, the insight of the suspension structure behind the load transfer pattern is revealed through the U^*-based design criterion introduced in Section 2. Finally, design modification can be proposed to the suspension structure based on the U^* analysis.

In this study, an in-house FEA-based program was developed for U^* calculation in Ansys Parametric Design Language [13]. Figure 7 shows the logic and the procedure

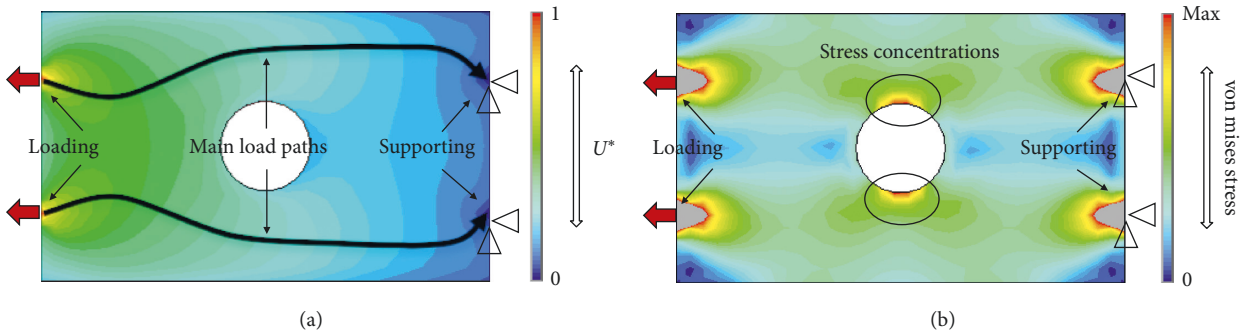

Figure 2: Load transfer analysis of a plate with a hole: (a) U^* distribution and main load paths; (b) von Mises stress distribution [9].

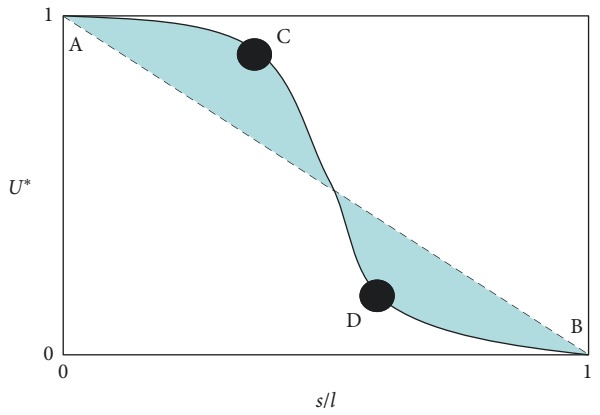

Figure 3: U^*-based design criterion to achieve uniform structural stiffness distribution [5].

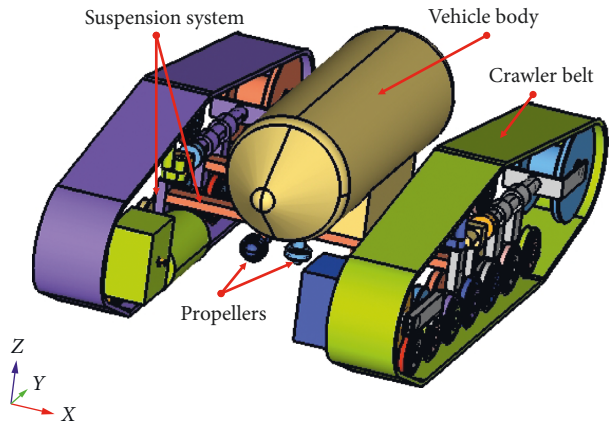

Figure 4: Computer-aided design model of a submarine vehicle (robot).

for the U^* algorithm development. The first step is the calculation of the total strain energy of the original system as shown in Figure 1(a). Secondly, by fixing an arbitrary node of the system and applying the same displacement to the loading point, the total strain energy of the modified system (Figure 1(b)) is calculated. Then, the U^* value of the arbitrary node can be computed through Equation (8). By repeating this step for each node of the system, the U^* distribution of the whole system is obtained. The total strain energy of the original system is only calculated once.

4. Results

Figure 8 presents the first three modal frequencies and shapes of the submarine vehicle. The first modal frequency of the vehicle, which is regarded as the natural frequency, is 37.6 Hz. The first modal shape of the vehicle is pitching oscillation, the second modal shape is heaving oscillation, and the third modal shape is rolling oscillation. The frequencies of the second and third modes can be also seen from Figure 8.

The U^* distribution of the suspension structure is shown in Figure 9(a). It shows the gravity force of the vehicle body is transferred through the horizontal part to the vertical part of the suspension. In Figure 9(b), the dashed white line illustrates the ideal situation of the U^* variation, while the solid blue line represents the actual U^* values along the marked load path in Figure 9(a). We can see the real U^* values along the load path deviate from the ideal situation, especially the circled area. Figure 9(b) indicates the U^* index decays sharply along the horizontal section of the suspension, while it drops slowly along the vertical section. The reason of this phenomenon is that the stiffness of the horizontal section of the submarine vehicle suspension is far lower than the vertical section. Therefore, increasing the stiffness of the horizontal section can effectively improve the overall stiffness of the suspension and thus raising the natural frequency of the whole vehicle. As discussed above, to increase the stiffness of the horizontal section of the suspension, its thickness was raised from 20 mm to 30 mm.

Figure 10(a) presents the U^* contour of the modified suspension, while Figure 10(b) shows the comparison of the U^* values along the load path between the modified and the original designs. From Figure 10(b) we can see that, in the horizontal section, the U^* values of the modified suspension are larger than the original design. It also can be seen that, at the joint between the horizontal and the vertical sections of the suspension, the U^* value of the modified structure is much closer to the ideal value compared to the original structure, i.e., with respect to the ideal condition, the deviation of the modified design is smaller than the original design. To quantitatively show the design improvement, ratios of the U^* values of the modified or the original design to the ideal U*

Table 1: Material properties of the major parts of the submarine vehicle.

Component	Material	Elastic modulus (MPa)	Poison's ratio	Thickness (mm)	Mass (kg)
Vehicle body	Aluminum	70,000	0.33	—	30
Vertical part of suspension (original)				20	5.23
Horizontal part of suspension (original)				20	3.57
Horizontal part of suspension (modified)				30	5.35

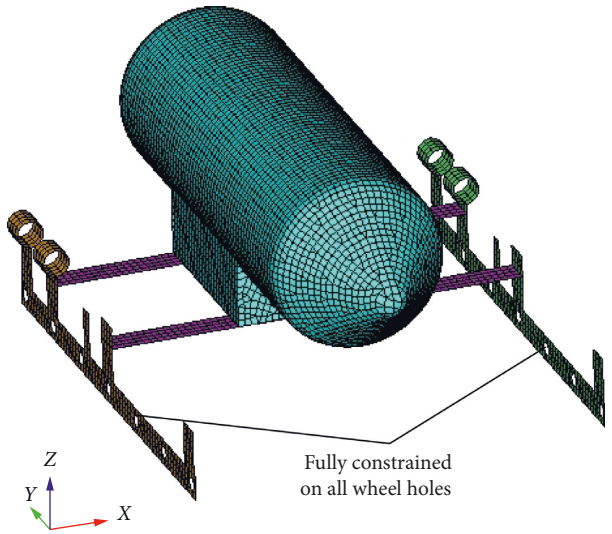

Figure 5: FEA model and mesh of the submarine vehicle structure for dynamic analysis.

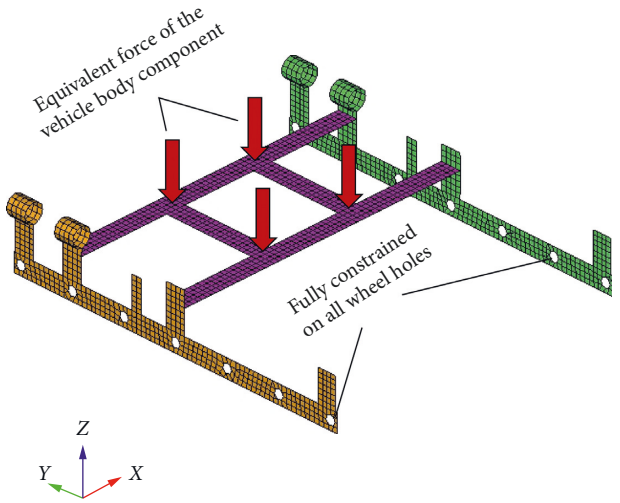

Figure 6: FEA model and mesh of the submarine vehicle structure for static U^* analysis.

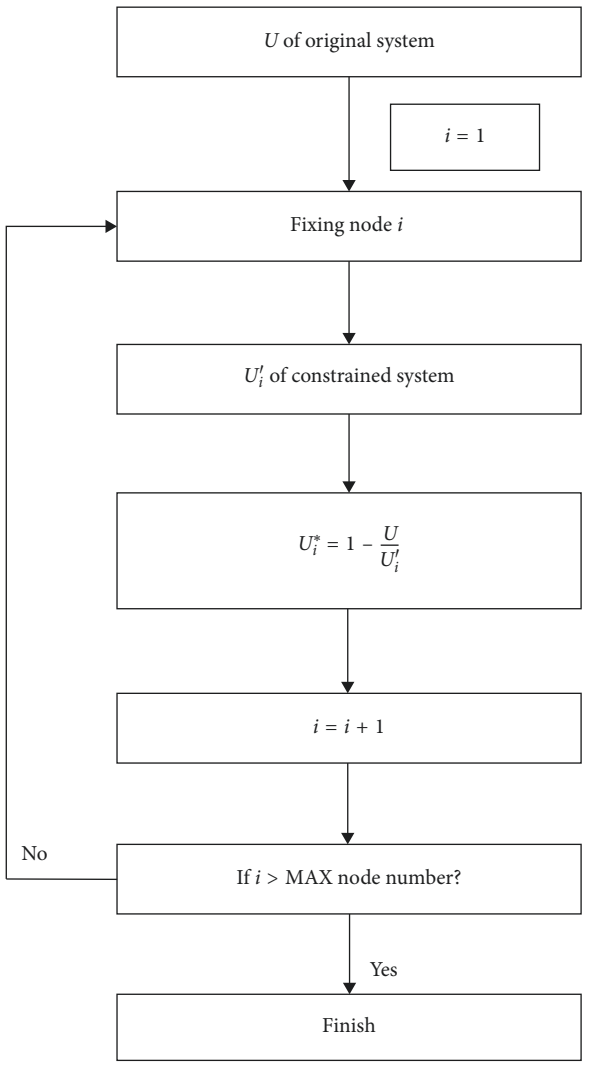

Figure 7: Flowchart to develop computer program for U^* calculation.

values (i.e., U^*_{design}/U^*_{ideal}) were obtained using the data points from Figure 10(b) and the mean and the coefficient of variation (COV) of the ratios were then computed, respectively, and illustrated in Table 2. The mean for the modified design is 1.01 comparing with 0.86 for the original design and the COV for the modified design is 17% instead of 33% for the original design. The improvement in terms of the U^* distribution indicates that the design modification narrowed the gap of the stiffness between the horizontal and the vertical sections of the vehicle structure. As a result, the stiffness distribution of the whole suspension is more uniform and the overall stiffness of the whole suspension is improved at the same time.

To see the effectiveness of the design modification, a new modal analysis was conducted to the submarine vehicle with the modified thickness in the horizontal section of the suspension. The modal shapes and the corresponding frequencies are depicted in Figure 11, where we can see that the first three modal frequencies of the modified vehicle were, respectively, improved by 43.5%, 40%, and 48% compared to the original design. Due to the design modification, the total weight of the

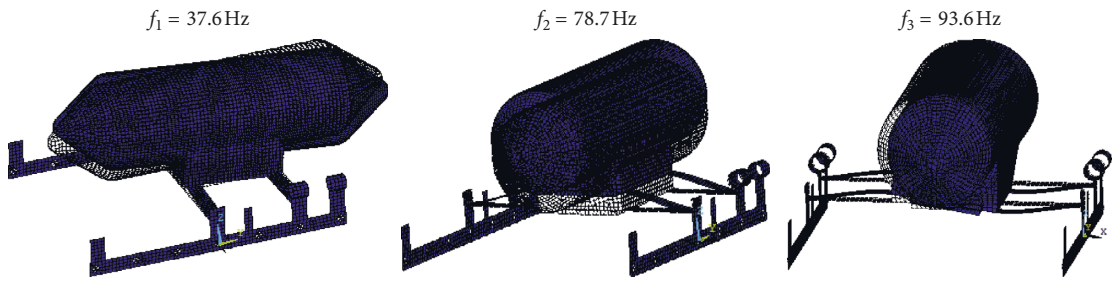

Figure 8: First three modal shapes and frequencies of the original submarine vehicle structure. (a) f_1 = 37.6 Hz. (b) f_2 = 78.7 Hz. (c) f_3 = 93.6 Hz.

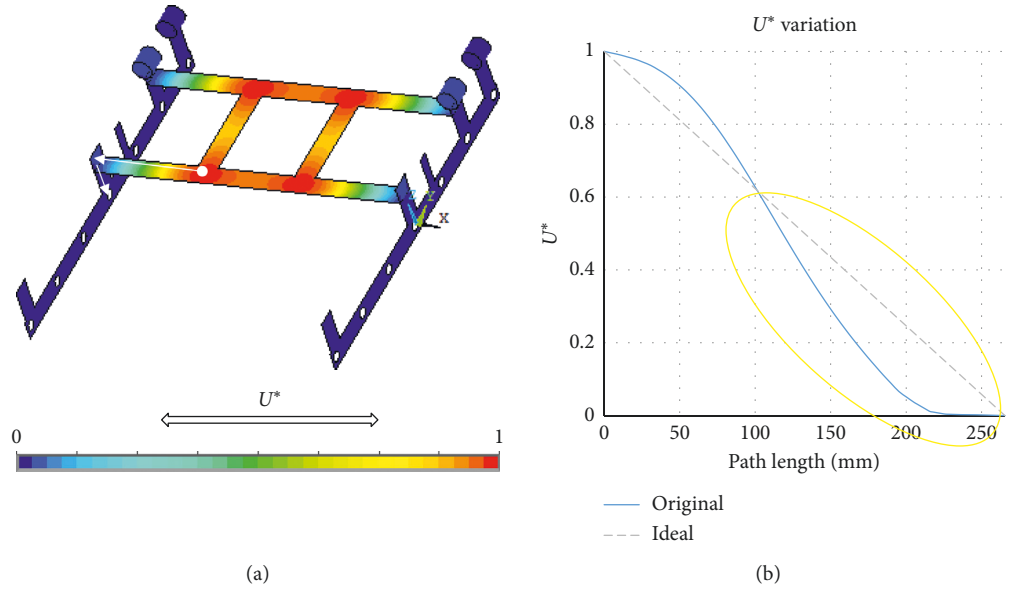

Figure 9: U^* analysis of the original submarine vehicle structure: (a) U^* contour of the structure; (b) U^* variation along a load path (white arrow).

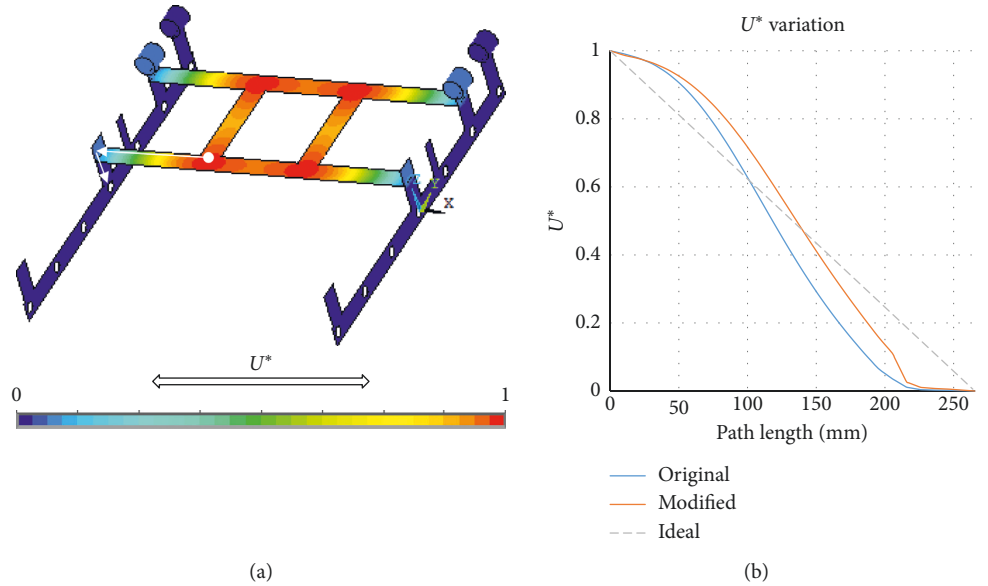

Figure 10: U^* analysis of the modified submarine vehicle structure: (a) U^* contour of the structure; (b) U^* variation along a load path (white arrow).

Table 2: Quantitative comparison with the ideal condition.

Design category	Mean of $(U^*_{design}/U^*_{ideal})$	COV of $(U^*_{design}/U^*_{ideal})$
Modified design	1.01	17%
Original design	0.86	33%

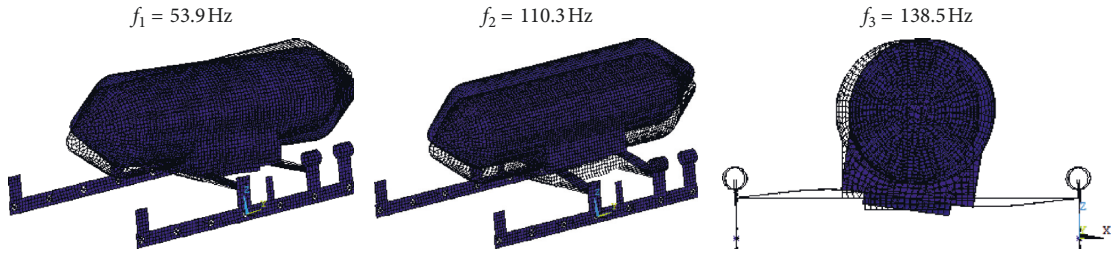

Figure 11: First three modal shapes and frequencies of the original submarine vehicle structure. (a) f_1 = 53.9 Hz. (b) f_2 = 110.3 Hz. (c) f_3 = 138.5 Hz.

submarine vehicle was only raised by 4.6% which was calculated based on the dynamic model shown in Figure 5.

5. Conclusion

The paper proposed a means for designing submarine vehicles or robots with the higher natural frequency in order to decrease the potential dynamic problems due to the road or seabed excitations.

With the help of the U^* index theory, the distribution of relative stiffness of a structure can be obtained, which provides designers with useful information in addition to the traditional FEA approach. The design modification based on the U^*-based approach considerably raised the natural frequency of the vehicle by adding a small amount of weight.

The results indicate that upgrade of overall stiffness of a structure can increase the structural natural frequency while the former can be improved by raising the uniformity of the stiffness distribution of the structure. Subjected to external forces or excitations, a structure with uniform stiffness distribution can realize the maximum overall structural stiffness based on a constant usage of material. The design criterion based on the U^* index theory is effective to evaluate and improve the uniformity of stiffness distribution of a structure.

Simply adding materials to each part of the vehicle structure can also improve its natural frequency. However, the increase of the structural weight may cause many other problems, e.g., fuel efficiency, weight limit, or control accuracy. This point can further highlight the usefulness of the proposed U^*-based approach in designing submarine vehicle structures with better dynamic performance. The work of this paper also implies that the U^* index theory is able to be applied for stiffness matching between different components of a vehicle system for addressing vibration problems.

Data Availability

All the computational data used to support the findings of this study are included within the article. It includes all the data related to the CAD model and the FEA model and the date of the modal analysis and U^* analysis. All the original data in this study are available upon request.

Conflicts of Interest

The authors declare that they have no conflicts of interest.

Acknowledgments

This work was supported by the NSFC (Natural Science Foundation of China) "Research on the Driving Stability of Undersea Observation Robot Steering on Slopes" (Grant no. 51605232). Some of the simulation work was also supported by the Natural Science Foundation of Zhejiang Province "Study on the Stability of Mobile Robot for Seafloor Exploration" (Grant no. LQ15E050004).

References

[1] H. Cheng and W. Li, "Reducing the frame vibration of delta robot in pick and place application: an acceleration profile optimization approach," *Shock and Vibration*, vol. 2018, Article ID 2945314, 15 pages, 2018.

[2] H. Hoshino, T. Sakurai, and K. Takahashi, "Vibration reduction in the cabins of heavy-duty trucks using the theory of load transfer paths," *JSAE Review*, vol. 24, no. 2, pp. 165–171, 2003.

[3] G. Verros, S. Natsiavas, and C. Papadimitriou, "Design optimization of quarter-car models with passive and semi-active suspensions under random road excitation," *JVC/Journal Vib. Control.*, vol. 11, no. 5, pp. 581–606, 2005.

[4] K. Takahashi and T. Sakurai, "Expression of load transfer paths in structures," *Transactions of the Japan Society of Mechanical Engineers Series A*, vol. 71, no. 708, pp. 1097–1102, 2005.

[5] Q. Wang, K. Pejhan, I. Telichev, and C. Q. Wu, "Demonstration of the effectiveness of $U*$ based design criteria on vehicle structural design," *Proceedings of the Institution of Mechanical Engineers, Part D: Journal of Automobile Engineering*, vol. 232, no. 8, pp. 995–1002, 2017.

[6] K. Takahashi, M. Omiya, T. Iso et al., "Load transfer ustar ($U*$) calculation in structures under dynamic loading," *Transactions of the Japan Society of Mechanical Engineers Series A*, vol. 79, no. 807, pp. 1657–1668, 2013.

[7] Q. Wang, K. Pejhan, I. Telichev, and C. Q. Wu, "Extensions of the $U*$ theory for applications on orthotropic composites and nonlinear elastic materials," *International Journal of Mechanics and Materials in Design*, vol. 13, no. 3, pp. 469–480, 2017.

[8] Q. Wang, I. Telichev, and C. Q. Wu, "A new load transfer index ($U*M$) with considering six degrees of freedom and its application in structural design and analysis," *Mechanics Based Design of Structures and Machines*, vol. 46, no. 4, pp. 410–424, 2018.

[9] Q. Wang, W. Zhou, I. Telichev, and C. Q. Wu, "Load transfer analysis of a bus bay section under standard rollover test using $U*M$ index $*$," *International Journal of Automotive Technology*, vol. 19, no. 4, pp. 705–716, 2018.

[10] H. Koboyashi, T. Naito, and Y. Urushiyama, "Study on similarity of load path distribution in body structure," *Honda R and D Technical Review*, vol. 23, no. 1, pp. 80–89, 2011.

[11] E. Wang, Y. Yoshikuni, Q. Guo et al., "Load transfer in truck cab structures under initial phase of frontal collision," *International Journal of Vehicle Structures and Systems*, vol. 2, no. 2, pp. 60–68, 2010.

[12] F. Beer, E. Johnston, J. Dewolf, and D. Mazurek, *Mechanics of Materials*, McGraw Hill Higher Education, New York City, NY, USA, 4th edition, 2006.

[13] ANSYS, *ANSYS® Academic Research, Release 18.0, Help System*, ANSYS, Inc., Canonsburg, PA, United States, 2017.